IEEE Photonics Journal
An IEEE Photonics Society Publication

Open Access

Analysis and Design of Chirped Fiber Bragg Grating for Temperature Sensing for Possible Biomedical Applications

Volume 10, Number 3, June 2018

Giovanna Palumbo
Daniele Tosi, ***Member, IEEE***
Agostino Iadicicco, ***Member, IEEE***
Stefania Campopiano, ***Member, IEEE***

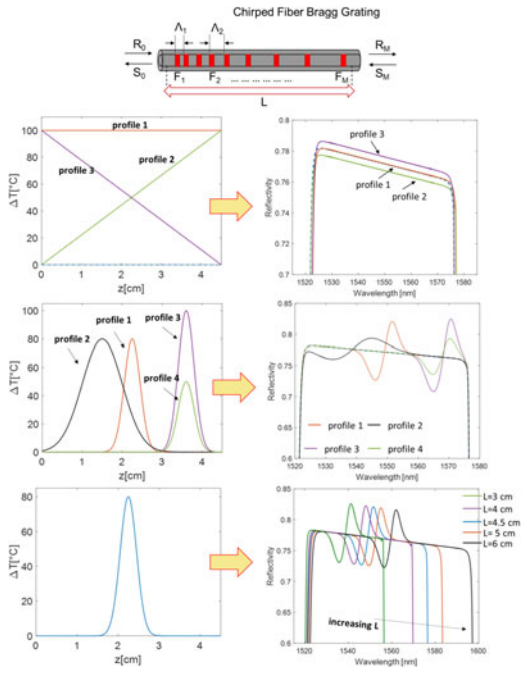

DOI: 10.1109/JPHOT.2018.2829623
1943-0655 © 2018 IEEE

Analysis and Design of Chirped Fiber Bragg Grating for Temperature Sensing for Possible Biomedical Applications

Giovanna Palumbo,[1] **Daniele Tosi**,[2,3] ***Member, IEEE***,
Agostino Iadicicco,[1] ***Member, IEEE***,
and Stefania Campopiano,[1] ***Member, IEEE***

[1]Department of Engineering, University of Naples "Parthenope," Naples 80143, Italy
[2]School of Engineering, Nazarbayev University, Astana 010000, Kazakhstan
[3]Laboratory of Biosensors and Bioinstruments, National Laboratory Astana, Astana 010000, Kazakhstan

DOI:10.1109/JPHOT.2018.2829623

Manuscript received March 1, 2018; revised April 16, 2018; accepted April 19, 2018. Date of publication April 24, 2018; date of current version May 15, 2018. The work of G. Palumbo, A. Iadicicco, and S. Campopiano was supported by the University of Naples "Parthenope" through the "Bando di sostegno alla ricerca individuale per triennio 2015–2017, Annualità 2016." Corresponding author: Giovanna Palumbo (e-mail: giovanna.palumbo@uniparthenope.it).

Abstract: In this paper, we present the design and analysis of chirped fiber Bragg grating (CFBG) sensors, optimized for temperature measurements. The transfer matrix method has been used to simulate the CFBGs and to study their thermal response. The simulations have been carried out with different temperature profiles in order to understand how the CFBG thermal response varies as a function of the grating design parameters and, thus, to optimize the design for the specific application. Finally, to assess the numerical simulations, a series of experimental tests was performed showing very good agreement.

Index Terms: Fiber Bragg grating, chirped fiber Bragg grating, temperature monitoring, biomedical applications

1. Introduction

In the last twenty years, fiber Bragg gratings (FBGs) widely demonstrated their sensing potentialities in several fields ranging from aerospace to civil engineering, from automotive to environmental monitoring [1]–[3], but above all, gained popularity in the medical sensing field [4]–[6].

In particular, among all the applications, our attention is focused on the growing use of fiber optic sensors for temperature monitoring in the medical field. Indeed, in addition to the aforementioned advantages of FBGs, we can also point out their small invasive impact, biocompatibility (ISO 10993 standard compliance) [7], and intrinsic absence of electrocution risk, chemically inertness, and the possibility of being easily inserted and embedded into surgical instruments, such as catheters and needles, and guided to a precise target during surgery. For these reasons, this type of sensors represents an optimal solution for thermal measurements during minimally-invasive medical technique [8]–[10]. Among these techniques, in last years, thermal ablation procedures for the treatment of small tumors are gaining attention, especially for patients who are not operative candidates or have particular medical problems or unresectable tumors. Thermal ablation can have several kind of sources as: radiofrequency, microwave, laser or high intensity focused ultrasound [11]–[15]. These

techniques use a miniaturized applicator, percutaneously inserted inducing a localized change of temperature (heating or cooling) in the tumor mass, while the surrounding healthy tissue should be preserved from the thermal damage [16]. An accurate and real time measure of thermal gradient is the key for the success of these procedures. The mortality rate of tumor cells is a function of the temperature value and of the duration of the ablation, i.e., the thermal dosimetry: in fast ablation processes, a heat temperature of 60 °C (for few seconds) must be reached for the instant cell death [8], [17].

On this line of argument, several research groups were interested in the use of fiber optic sensors for temperature measurement during thermal treatments. In particular, Tosi *et al.* [18] have reported the use of distributed fiber optic sensor system based on fast demodulation of Rayleigh scattering pattern during radiofrequency thermal ablation in porcine phantom. The sensing system is able to measure temperature gradients in excess of 5 °C/mm; another of their work, is based on thermal monitoring during radiofrequency ablation through a fiber Bragg grating array having 1 sensor/cm density installed on a RF needle [19]. Tests on kidney and liver rabbit undergoing hyperthermia treatment, were carried out using a fiber Bragg grating system making a comparison with a commercial fluoroptic thermometry system [20]. Samset at al. [21], developed a distributed fiber Bragg grating sensor system for use in biological tissue. Experiments were conducted during cryoablation of porcine liver in vivo. The system yielded a temperature profile with 6.5 mm spatial resolution and 5 s time resolution. Our research group worked on the development of a FBG system integrated with a commercial radiofrequency probe, too. Experiments on ex-vivo animal kidney and liver were conducted and a real time, multipoint measurement with a temperature resolution of 0.1 °C and a spatial resolution of 5 mm was achieved [10], [22]. Another study was carried out on the application of two FBG arrays placed close to the RF applicator and over the sub-lethal isotherm [23], [24]. Comparisons between the measurements of these two arrays, positioned in different positions after several RF discharges, were made.

However, despite their above-mentioned advantages, the FBGs sensors present limitations related to a point measurement. Indeed, the commercial standard FBGs have a typical length (1–10 mm) that could be excessive for these kinds of applications. This limitation can be overcome through multiplexing techniques, leading to a quasi-distributed sensor (only few works are available [25], [26]).

An interesting alternative, for thermal monitoring in medical applications, is based on Chirped FBG (CFBG), where it is possible to associate the position of a thermal pulse along the grating region of the CFBG sensor. With this type of sensors, it is possible to improve the spatial resolution achieved with standard FBGs, with a sensitive structure covering a length of centimeters. CFBGs, differently from standard FBGs, which have a spatially periodic modulation of the core refractive index, present non-periodic pitch [27]–[29]. CFBGs behave like a chain of FBGs inside an optical fiber, where each grating reflects one specific wavelength, returning a broadband spectrum that depends on several parameter as temperature, strain, applied along the whole grating length [30], [31]. Thanks to their specific features, CFBGs are now widely used in optical communication systems [32], [33] and in sensor applications, i.e., in mechanical engineering for strain and crack detection [34], [35].

One of the first work on CFBG was conducted by Won at al. in 2004 [36]. They evaluated the effect of a temperature gradient on CFBG with 3 nm band, using the transfer matrix method to evaluate temperature change, position and width of localized heating applied to the grating. Tosi et al. in [37], proposed first studies for the demodulation process of CFBG spectrum in order to discriminate a temperature effect along the fiber during medical procedure and to obtain a distributed thermal map. Through the use of a decoding algorithm, a linearly chirped FBG for distributed thermal measurement during radiofrequency thermal treatments was used. In another work, the authors proposed a method based on an iterative optimization that aims at minimizing the mismatch between the measured CFBG spectrum and a CFBG model based on coupled mode theory (CMT) perturbed by a temperature gradient. In the demodulation part, the authors simulate different temperature distribution patterns with MonteCarlo approach on simulated CFBG spectra. Experiments and simulations have been carried out with different temperature gradient profile [38].

In this work, we present a study of CFBG dependence on grating parameters showing that they can be optimized for the specific application. In particular, our attention was focused on the use of CFBG with wide bandwidth, about 56 nm, in order to increase the length of the sensor and have a greater ability to read the temperature pattern during thermo-ablation medical procedures. Several simulations were performed, with the aim of analyzing the response of CFBG sensor as function of the grating parameters (such as length and chirp rate). We studied the CFBG response when subjected to different thermal gradients, analyzing how it varies as function of the design parameters. The study leads to a precise knowledge of the CFBG thermal sensing behavior, so that it is possible to design a proper custom CFBG sensor for the specific needs. Moreover, this approach has been validated through a series of experimental tests showing that experimental and simulated results are in very good agreement.

2. Numerical Analysis

In this section, we describe the transfer matrix method used for the study and analysis of the chirped FBG sensors.

An FBG sensor is an intrinsic sensor, produced by various techniques and formed by a periodic modulation of the index of refraction of the fiber core along the longitudinal direction. The FBG principle of operation is based on the coupling between the forward and the backward propagating core modes. When light propagates through a fiber with a Bragg grating, a reflection phenomenon for a narrow range of wavelengths occurs. In particular, the reflected spectrum is centered at a specific value, called Bragg wavelength. This behavior makes FBG sensors similar to a notch reflection filter, allowing the selection of a particular wavelength and bringing it back into reflection.

2.1 The Transfer Matrix Method

Chirped fiber Bragg gratings are characterized by a grating period Λ that changes along the fiber length, resulting in light reflected at different wavelengths. Indeed, as the grating period varies along the axis, different wavelengths are reflected by different portions of the grating. Therefore, the resulting spectrum is wide and it can be seen as function of the position along z-axis of the fiber [27], [39]. To realize the non-uniform structure of CFBG, and to obtain the UV interference photo-imprinted pattern, a phase mask having a specific chirped period is used [28], [40]. For instance, in order to obtain a linearly chirped FBG, a phase mask with linearly varying pitch was employed in the UV writing set-up exposing the fiber core to a chirped light interference pattern. The sensor thus obtained, has the start pitch and the chirp given by the phase mask characteristics [28].

Generally, the simulation of fiber gratings (uniform and non- uniform) is usually conducted by using the transfer matrix method (TMM) [30]. This technique is based on CMT, which is a simplified theory derived from Maxwell's equations and analyze the wave propagation and interactions with materials in optical waveguide [41].

This approach follows a piecewise-uniform process, in which the grating is divided into a certain number of uniform pieces. In particular, the CFBG, with length L, is divided into M uniform sections (the larger the number of M, more accurate this method will be), as it is shown in Fig. 1. This method is simple to implement, since the closed-form solutions for each uniform piece are combined by multiplying the matrixes associated with the pieces [30], [42].

The propagation of the incident light wave through each uniform section *i* is described by a transfer matrix F_i, which is described below:

$$\begin{bmatrix} R_i \\ S_i \end{bmatrix} = F_i \begin{bmatrix} R_{i-1} \\ S_{i-1} \end{bmatrix} = \begin{bmatrix} F_{11} & F_{12} \\ F_{21} & F_{22} \end{bmatrix} \begin{bmatrix} R_{i-1} \\ S_{i-1} \end{bmatrix} \tag{1}$$

where R_i and S_i are the field amplitudes after propagating through the section *i,* while R_{i-1} and S_{i-1} are the field amplitudes before the section *i*. It is defined as a 2×2 matrix for each uniform section and then, it multiplies all of these together in order to obtain a single 2×2 matrix that describes

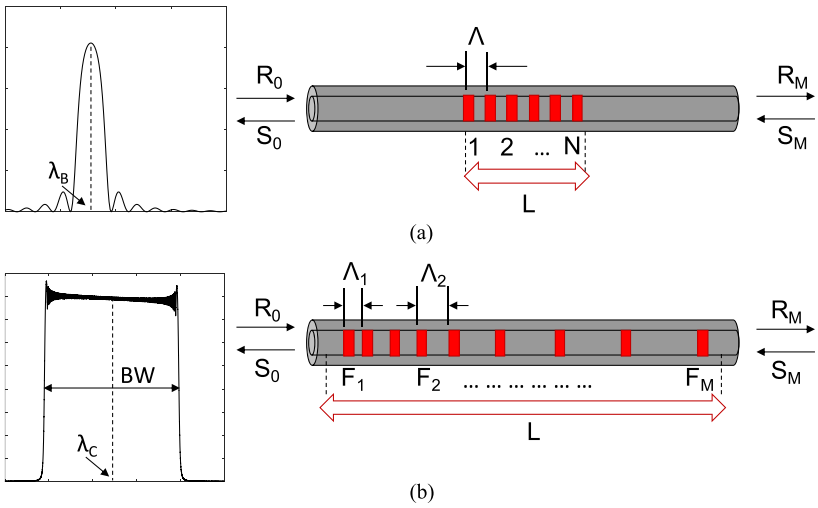

Fig. 1. Scheme of the grating and respective spectrum (a) uniform grating; (b) non-uniform grating.

the whole grating [30], [43]. The output amplitude is shown in the (2) below:

$$\begin{bmatrix} R_M \\ S_M \end{bmatrix} = \boldsymbol{F} \begin{bmatrix} R_0 \\ S_0 \end{bmatrix}; \quad \boldsymbol{F} = \boldsymbol{F_M} \cdot \boldsymbol{F_{M-1}} \cdot \ldots \ldots \boldsymbol{F_i} \cdot \ldots \ldots \boldsymbol{F_1} \tag{2}$$

The elements in each transfer matrix have the following expression:

$$F_i = \begin{bmatrix} \cosh(\gamma_B \Delta_z) - i\frac{\hat{\sigma}}{\gamma_B}\sin(\gamma_B \Delta_z) & -i\frac{\kappa}{\gamma_B}\sinh(\gamma_B \Delta_z) \\ i\frac{\kappa}{\gamma_B}\sinh(\gamma_B \Delta_z) & \cosh(\gamma_B \Delta_z) + i\frac{\hat{\sigma}}{\gamma_B}\sin(\gamma_B \Delta_z) \end{bmatrix} \tag{3}$$

where Δ_z is the length of the ith section. The coupling coefficient $\hat{\sigma}$ and κ are the local values in the ith section [27], [30], while $\gamma_B = \sqrt{\kappa^2 - \hat{\sigma}_2}$ is the imaginary part for which $|\hat{\sigma}| > \kappa$.

The output amplitudes for the non-uniform FBG are obtained by applying the boundary conditions, $R_0 = R(L/2) = 1$, and $S_0 = S(L/2) = 0$.

Among the parameters for the realization of a CFBG spectrum, the definition of the correct chirp profile is essential. The term for the chirp, in linear case can be explicated as:

$$\frac{1}{2}\frac{d\phi}{dz} = -\frac{4\pi n_{eff} z}{\lambda_D^2}\frac{d\lambda_D}{dz} \tag{4}$$

where the term $d\lambda_D/dz$, is the measure of the rate of change of the design wavelength with position in the grating, usually given in units of nanometers/centimeters [30]. In the following, we will refer to this term as the chirp rate.

2.2 Apodization Profiles

Power reflectivity characteristics can be made more stable by applying apodization profile to fiber grating. Apodization consists of a variation of the modulation depth along the grating length. Therefore, the apodized grating has an important role in order to suppress the side lobes, which are due to multiple reflections at the grating ends [30], [44].

The effect of apodization, is reported in the $\overline{\delta n_{eff}}$ parameter [30]:

$$\overline{\delta n_{eff}}(z) = \overline{\delta n_{eff}}\, f(z) \tag{5}$$

where $\overline{\delta n_{eff}}$ is the refractive index modulation peak and $f(z)$ is the apodization profile.

Different grating apodization profiles can be used, for example Uniform (no apodization), Hyperbolic Tangent and Gaussian, which are described as a function of spatial distance as

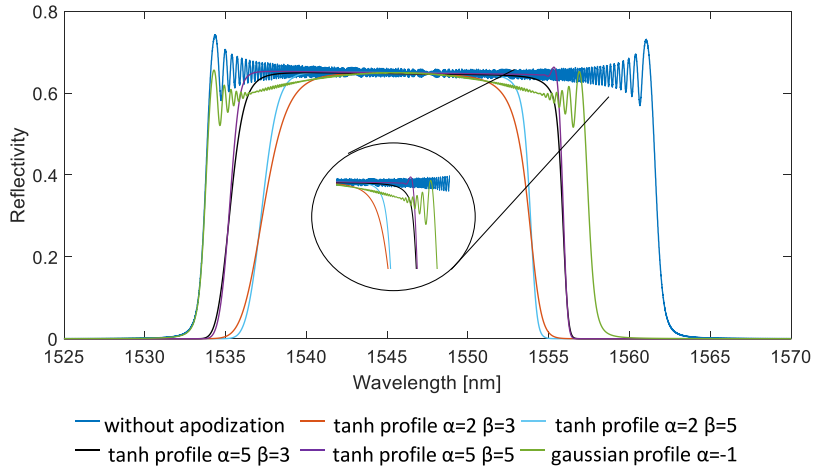

Fig. 2. Spectral effects of different apodization profiles.

[30], [44], [45]:

$$\text{Uniform (no apodization)} \qquad f(z) = 1 \tag{6}$$

$$\text{Tanh Profile} \qquad f(z) = \frac{1}{2}\left[1 + \tanh\left(\beta\left(1 - 2\left|\frac{2z}{L}\right|^{\alpha}\right)\right)\right] \tag{7}$$

$$\text{Gaussian profile} \qquad f(z) = \exp\left[-\alpha\left(\frac{z - L/2}{L}\right)^2\right] \tag{8}$$

In Fig. 2, it is reported the effect on the CFBG spectrum of different apodization profiles, as obtained from simulations using the following parameters: $L = 3$ cm; $\overline{\delta n_{eff}} = 5 \cdot 10^{-4}$; $\Lambda = 530$ nm; chirp rate $(d\lambda_D/dz) = 4$ nm/cm. In the figure, it is shown how by applying the proper apodization profile, it is possible to attenuate the presence of side lobes and obtain a cleaner profile. As it will be shown in the following, in order to obtain a CFBG spectrum useful for biomedical applications, the hyperbolic tangent profile will be considered.

3. Temperature Characterization

In this section, we present the study of the dependence of temperature sensitivity of a CFBG sensor on the design parameters. In detail, we performed various simulations by using TMM method, changing the main parameters and evaluating the effects on the CFBG sensor response. The final aim is the design of the chirped parameters in order to obtain the proper sensitivity to temperature profile.

3.1 CFBG Response to Linear Temperature Profile

By using the TMM method, several simulations with different temperature profiles applied to CFBG were performed. The simulations were made on a linear chirp CFBG with parameters similar to the commercial one used for the experimental comparison (as it will be shown in the next session), that are: $L = 4.5$ cm; $\overline{\delta n_{eff}} = 7.8 \cdot 10^{-4}$; $\Lambda = 524$ nm; chirp rate $(d\lambda_D/dz) = 6.73$ nm/cm. Moreover, a tanh apodization profile was applied with the following parameters: $\alpha = 7$ and $\beta = 5$.

In Fig. 3, the results of three different simulations are reported, obtained by applying three different linear temperature profiles along the whole length of the CFBG. In particular, as it is shown in Fig. 3(a):

- Profile 0): without temperature profile applied,
- Profile 1): a temperature constant profile of 100 °C,

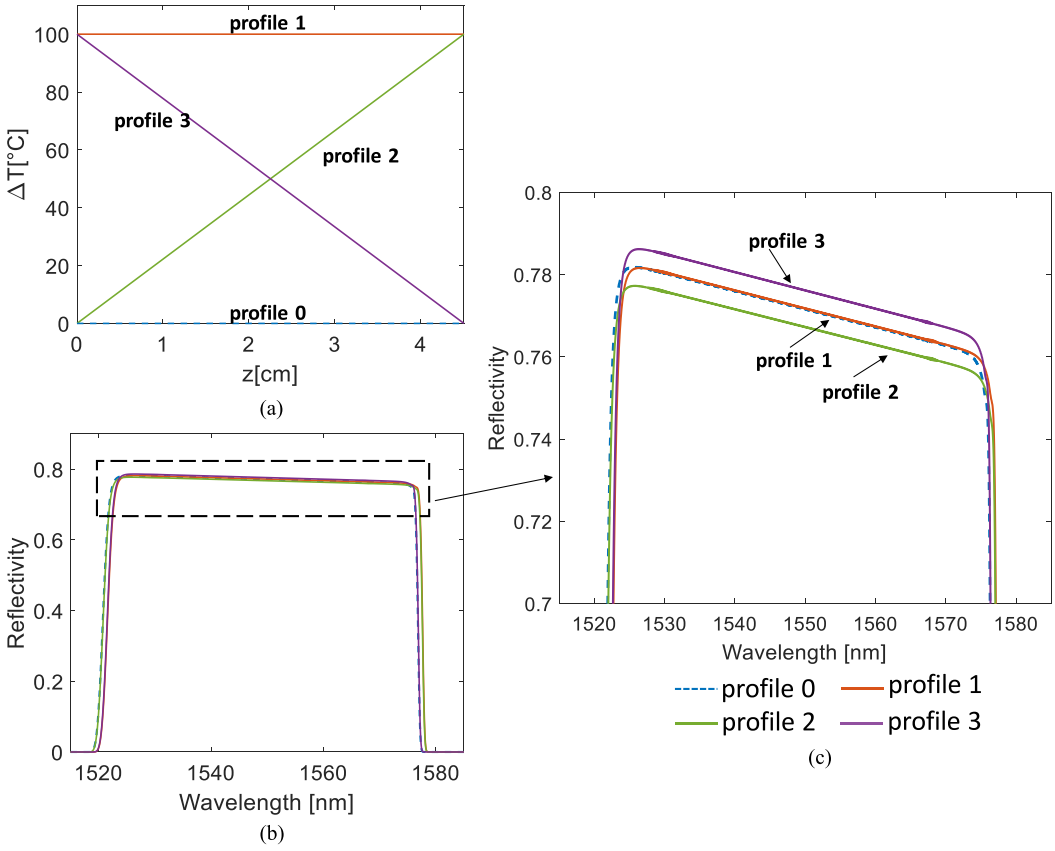

Fig. 3. Simulation results of three linear temperature gradients (a) temperature profile; (b) corresponding CFBG spectra; (c) zoom of CFBG spectra.

- Profile 2): a temperature profile linearly varying from 0 to 100 °C,
- Profile 3): a temperature profile linearly varying from 100 to 0 °C.

The CFBGs spectra simulated, have a band between 1521 nm and 1578 nm with a reflectivity around 0.77.

As it is possible to see from Fig. 3(b) and even more in detail from zoom in Fig. 3(c), the application of a linear temperature profile does not change the shape of the spectrum of the CFBG sensor, but the effects are only a uniform change in the reflectivity baseline and a variation of CFBG band.

In particular, for the constant profile, (profile 1) it is possible to see, due to a positive temperature gradient, a red shift of about 0.82 nm of the entire CFBG spectrum without a change in bandwidth (which is of 56 nm), while no change in the baseline of reflectivity is noticeable. For the profile 2, ranging from 0 to 100 °C, there is a shift of the falling edge, at the points of application of the maximum temperature (positive shift of 0.78 nm respect to spectrum without solicitation) with a consequent increase in band of 0.73 nm.

In this simulation, unlike the previous case, there is a small variation in reflectivity, as it can be seen from the zoom of Fig. 3(c), there is a decrease in reflection of about 0.0044 along the whole CFBG band. Symmetric behavior is observed for profile 3 (ranging from 100 to 0 °C): a shift of rising edge (0.78 nm respect to spectrum without solicitation) with a decrease in the bandwidth of 0.73 nm, moreover, even in this case, a slight variation of reflectivity is observed. As the applied profile has an opposite trend to the previous one (profile 2), i.e., the temperature gradient ranges from positive values (100 °C) to 0 °C, the baseline relative to the reflectivity value undergoes a slight increase of about 0.0044 along the whole CFBG band. In conclusion, as from the results of profile 2 and 3, an increase in the bandwidth for positive linear temperature gradients and analogously a reduction in the bandwidth for negative ones is shown. It is worth to note that not constant temperature profiles

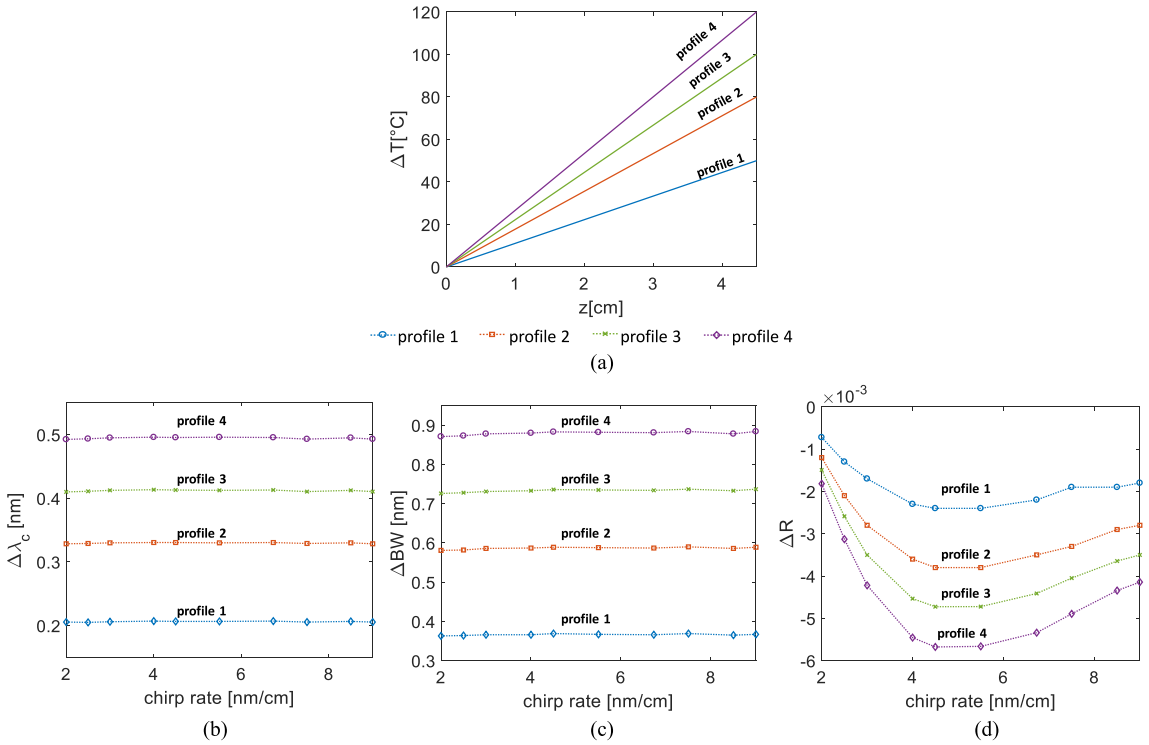

Fig. 4. Simulation results as function of chirp rate (a) temperature profile applied; (b) variation of λ_C; (c) variation of BW; (d) variation of reflectivity.

change the chirp rate that, as also confirmed in the following, directly influences the reflectivity in a nonlinear way. Indeed, profile 4 is uniform and thus, doesn't change the reflectivity. Whereas, profile 2 induces a chirp rate increase that causes a reflectivity decreases while profile 3 induces a chirp rate decrease that causes a reflectivity increases.

From the spectrum analysis, and in particular by the analysis of the variation of the central wavelength (in the middle point of BW -Fig. 1) between the reference and the solicited spectrum, it is noted that the sensor so designed, has a thermal sensitivity of 8.5 pm/°C.

In order to characterize the behavior of a CFBG spectrum subjected to a thermal solicitation, simulations by varying the design parameters of the CFBG sensor were made. In particular, starting from the previous simulated sensor ($L = 4.5$ cm; $\overline{\delta n_{eff}} = 7.8 \cdot 10^{-4}$; $\Lambda = 524$ nm), a series of simulations by changing the chirp rate, were performed. Four different linear temperature profiles have been applied, and for each of them, simulations have been made by varying the chirp parameter (Fig. 4).

In Fig. 4(a), are reported the linear temperature profiles applied, while in Fig. 4(b) and (c), the variation of λ_C and *BW* (parameters evaluated as shown in Fig. 1) with respect to the situation without temperature applied, as function of the variation of the chirp are shown; in Fig. 4(d), the variation of reflectivity as calculated at the center of the bandwidth, with respect to a condition without temperature applied as function of the chirp rate for all four applied linear profiles, is presented.

In Fig. 4(b) and (c), it is possible to see how the chirp rate variation does not affect the variation of the central wavelength and bandwidth, where a linear trend is observed. However, different is the reflectivity behavior (Fig. 4(d)) where the trend with respect to the chirp is not linear, but decreases as the chirp coefficient increases until to a value of 5.5 nm/cm, then slightly increases. Therefore, for chirp values between 4.5 and 5.5 nm/cm the maximum reflectivity variability is detected.

As a result, in order to have a greater temperature sensitivity in terms of grating reflectivity changes, it is convenient to choose CFBGs with a chirp rate between 4.5 and 5.5 nm/cm whereas central wavelength shifts and bandwidth variations slightly depend on the chirp rate.

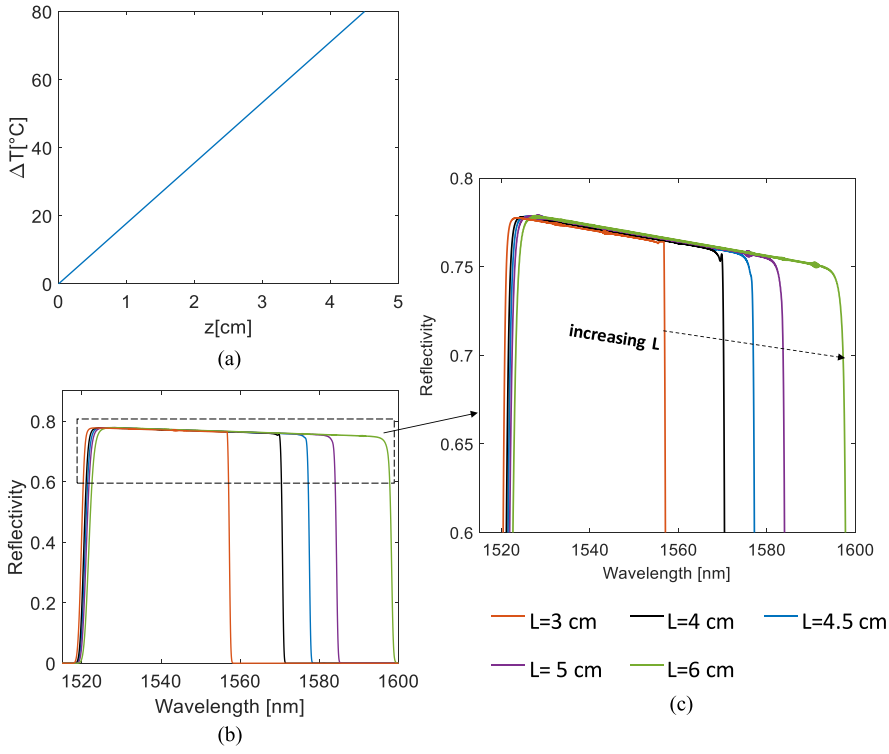

Fig. 5. Simulation results by applying a linear temperature gradient: (a) temperature profile; (b) CFBG spectra with different grating length; (c) zoom of CFBG spectra with different grating length.

A further simulation was performed by varying the length of the CFBG, applying a linear temperature profile on them, as it is shown in Fig. 5. The applied profile is linear and covers the entire length of the CFBG, with a maximum of 80 °C at the end of the grating (Fig. 5(a)).

The parameters used to simulate the CFBG spectrum are: $\overline{\delta n_{eff}} = 7.8 \cdot 10^{-4}$; $\Lambda = 524$ nm and chirp rate $(d\lambda_D/dz) = 6.73$ nm/cm. In Fig. 5(b) and (c), the trend of the reflectivity by varying the grating length is shown. As it is evident from the zoom in Fig. 5(c), as the grating length increases, an increase in the bandwidth of the CFBG is present. In particular, 1 cm increase in the length of the grating, leads to an increase in bandwidth of about 12 nm. Moreover, the applied profile leads to a change of reflectivity of 0.003 (compared to the spectrum without profile applied) for all simulated spectra. Similar behavior, regarding the bandwidth is observed: for all CFBG sensors simulated, there is a small increase in bandwidth following the application of a high temperature at the end of the grating (as already noted from the previous test in Fig. 3). The bandwidth increase is of about 0.62 nm for all the gratings, so it can be concluded that the length of CFBG does not affect the response and the sensitivity of the sensor to a linear temperature profile, and, thus, it is a parameter not useful in the temperature sensitivity optimization process.

3.2 Simulations With Gaussian Thermal Gradient

In order to apply the CFBG sensors to the thermal monitor field, we wanted to study the effects of a Gaussian profile (which is the profile generated by Radiofrequency and Laser Ablation (RFA – LA) thermo-ablation procedures [15], [16]) on a chirped fiber Bragg grating sensor.

In Fig. 6, the results of the simulations are presented. In Fig. 6(a), four Gaussian temperature profiles are applied at different points of the CFBG grating; the applied temperature gradients differ for width and maximum temperature. The sensor parameters used for simulations are: $L = 4.5$ cm; $\overline{\delta n_{eff}} = 7.8 \cdot 10^{-4}$; $\Lambda = 524$ nm and chirp rate $(d\lambda_D/dz) = 6.73$ nm/cm. From the zoom of Fig. 6(c), it is seen that a Gaussian profile, regardless of the point of application, does not change the CFBG

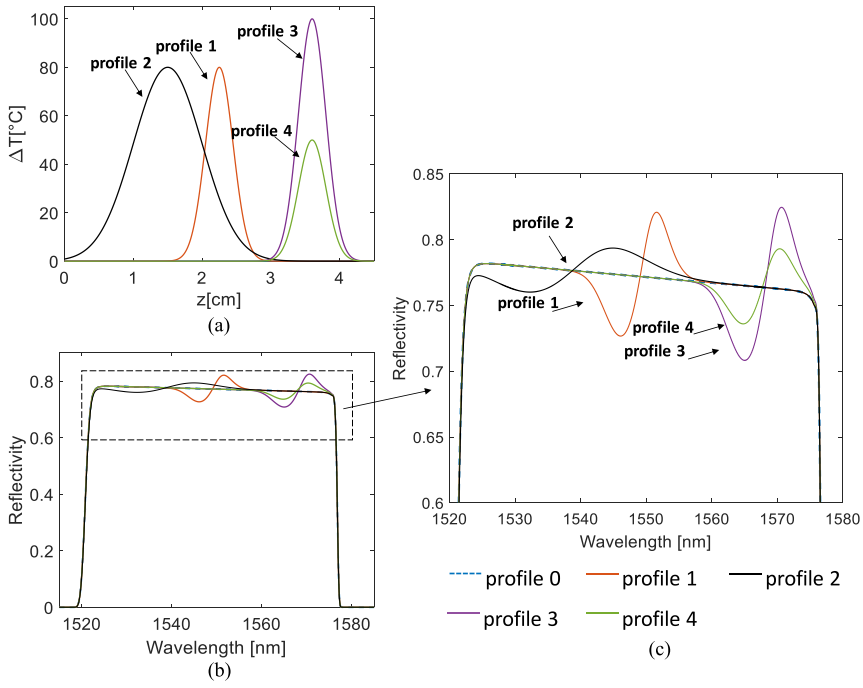

Fig. 6. Simulation results for four Gaussian temperature gradients: (a) temperature profile; (b) CFBG spectra; (c) zoom of CFBG spectra.

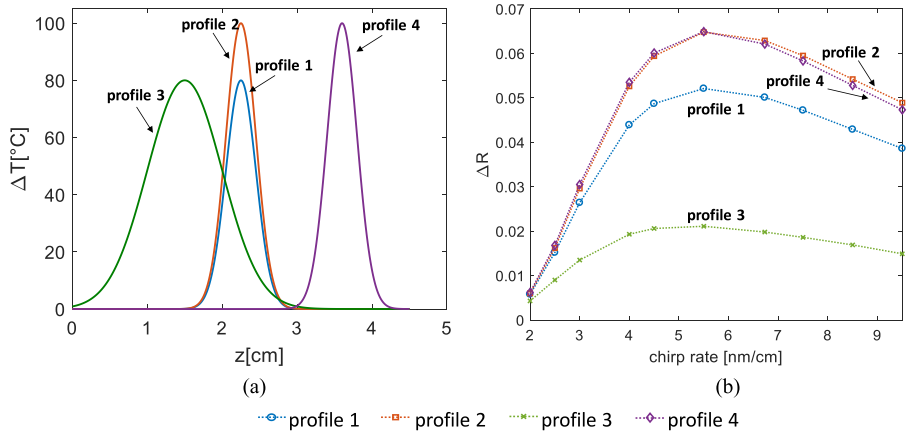

Fig. 7. Simulation results as function of the chirp rate: (a) applied temperature profile; (b) variation of Reflectivity vs chirp rate.

band but leads to a change in the shape of the baseline of reflectivity. In particular, the application of a Gaussian profile leads to the formation of a symmetric negative and positive peak, at the center of these two peaks, we find the maximum temperature of the Gaussian profile simulated.

Another important aspect is that, a profile applied to the most part of grating, gives a small contribution most widely distributed on the along the CFBG spectrum, on the contrary, as seen on profile 3, a very narrow Gaussian profile with a maximum of 100 °C has a prominent positive and negative peak. In fact, profiles applied at the same point of the grating with equal width, but maximum different (profile 3 and profile 4), show a reflection spectrum with different positive and negative reflectivity peaks, depending on the maximum temperature applied.

In Fig. 7, four different Gaussian temperature profiles by varying chirp rate are applied. The parameters used to simulate the CFBG were: $L = 4.5$ cm; $\overline{\delta n_{eff}} = 7.8 \cdot 10^{-4}$; $\Lambda = 524$ nm. In

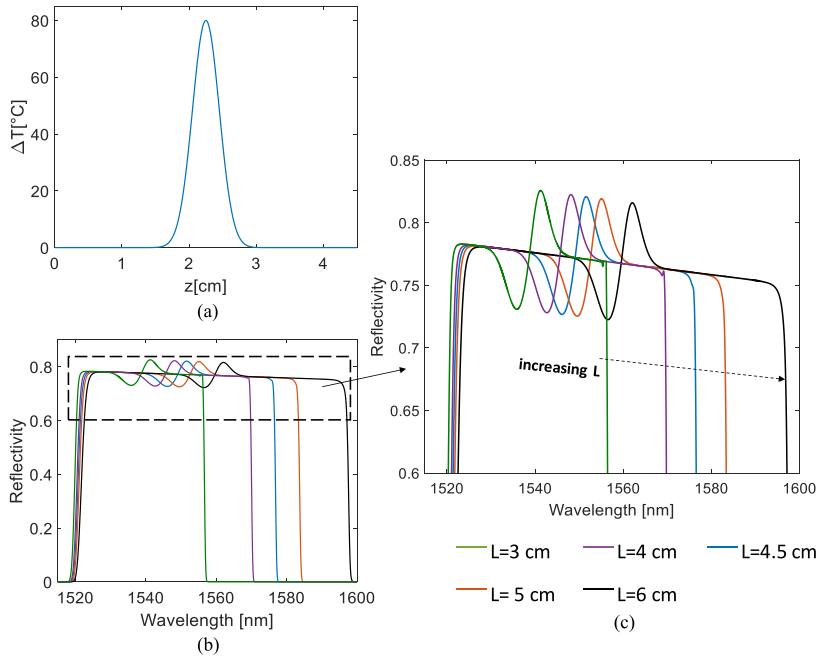

Fig. 8. Simulation results by applying a Gaussian temperature gradient: (a) temperature profile; (b) CFBG spectra for different grating length; (c) zoom of CFBG spectra.

Fig. 7(a), the applied Gaussian temperature profiles are represented, while in Fig. 7(b), the trend of reflectivity with respect to the variation of the chirp is reported. The trend of ΔR with respect to the chirp rate, is always increasing for all profiles applied. For profile 3, the variation of reflectivity is less significant than the other profiles, because profile 3 is applied to a larger grating surface. The profile 2 and profile 4, which have the same characteristics, but applied at different points, have the same variation of ΔR in relation to the chirp rate, therefore the variation is not affected by the application point of the profile, but only by the temperature profile characteristic. This behavior is also confirmed for the profile 1, which has a minor temperature variation, because its maximum is smaller than the other two profiles (80 °C respect to 100 °C). In conclusion, from the analysis of the Fig. 7(b), it is evident that the maximum sensitivity value is for a chirp rate between 5 and 6 nm/cm.

In order to further monitor the behavior of a simulated CFBG, when a Gaussian profile is applied, another simulation was performed. In the Fig. 8, it is shown the response of the CFBG profile respect to the variation of the grating length. The Gaussian profile shown in Fig. 8(a), is applied to the center of the sensor with a maximum temperature of 80 °C. The parameters used for this simulation are the same as the previous one, except for the length that has been varied.

As already seen in the simulation shown in Fig. 5, as the length of the grating increases, also the bandwidth of the sensor increases. Moreover, in the zoom of Fig. 8(c), it is noted that, the shape of the spectral baseline variation is the same for all the gratings, hence the length does not influence the variation of reflectivity. Indeed, for all the spectra there is a variation of ΔR of about 0.06 nm, while the bandwidth remains unchanged respect to the spectrum without solicitation.

From the previous analysis, it is possible to conclude that the chirp rate is the main parameter of the CFBG useful for the temperature sensitivity optimization process, whereas other parameters like grating length do not improve the temperature sensitivity.

4. Experimental Validation

In this section, we compare the behavior of a commercial CFBG with a CFBG simulated, assuming similar spectra. From the experimental point of view, the sensor was stimulated by applying a temperature gradient in different points of the grating.

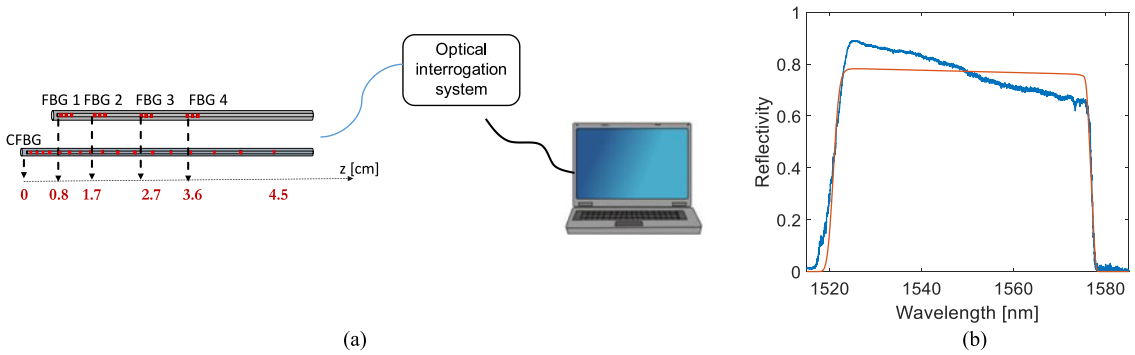

Fig. 9. (a) Schematic of the optoelectronic setup; (b) comparison between the experimental spectrum and the simulated spectrum.

The parameters chose for the simulation are: $L = 4.5$ cm; $\overline{\delta n_{eff}} = 7.8 \cdot 10^{-4}$; $\Lambda = 524$ nm; chirp rate $(d\lambda_D/dz) = 6.73$ nm/cm.

For experimental tests, a specific setup was made (as it is illustrated in Fig. 9(a)). In particular, a commercial sensor with linear chirp was used. The CFBG under test is written on a single-mode fiber SMF-28 and has 4.5 cm active length, with a bandwidth of about 56 nm, from 1521 nm to 1577 nm. Alongside the CFBG sensor, four FBG standard of 0.5 cm length were used, in order to monitor the temperature trend at different points of the chirped sensor. So, arranged sensors were connected to an optical interrogation system used to measure the FBGs reflected signal. This system, included a tunable laser operating in the range of 1500 to 1600 nm that is equipped with eight optical channels allowing for simultaneous measurement of a large number of sensors (up to 25 for each channel). The detector measured the Bragg wavelengths with a resolution of 1 pm with a minimum sampling frequency of 1 Sample/s. Finally, the spectra acquired were analyzed through a personal computer.

The comparison between the numerical and experimental spectra at uniform room temperature is reported in Fig. 9(b). As it can be seen from Fig. 9(b), the spectrum of commercial CFBG shows a decreasing baseline, this is because the photosensitivity of the grating tends to shrink during writing, and thus the reflectivity decreases. In a future set-up, it is possible to consider the use of a dynamic Waveshaper filter to equalize and straighten the spectrum of CFBGs, so that the commercial sensor spectrum can match that of the simulation.

In Fig. 10, it is reported the experimental test performed. The sensors were placed on a rigid support and the application of the temperature gradient was carried out using a welder. In particular, the tip of the welder was applied at the beginning of the chirp, at the free end of the sensor (as shown in Fig. 10(a)). In Fig. 10(b), the commercial CFBG sensor response is reported. In particular, in the inset of Fig. 10(b), the trends of the two temperature profiles applied, are reported. These profiles have been measured by using the data provided by the four FBG standard sensors. As it is possible to note, the application of a ΔT leads to a positive shift of the wavelengths. Indeed, the application of ΔT, has led to a shift of the rising edge, while no shift of the falling edge or the baseline of the reflectivity are evident. For the profile 1, having a maximum temperature of 120 °C on the free tip of the chirped sensor, there is a shift of the rising edge of about 0.94 nm with a consequent reduction in the bandwidth from 56.22 nm to 55.30 nm, with respect to the spectrum without temperature profile applied. While for profile 2, with a maximum temperature variation of 80 °C, minor variations are recorded: i.e., a positive shift of the rising edge of 0.69 nm, with a reduction in bandwidth from 56.22 nm to 55.54 nm.

In Fig. 10(c), the response of the simulated CFBG sensor with the application of the same two temperature profiles obtained from the experimental test, is reported. As it can be seen, even in this case, there is only a shift of the rising edge: for the profile 1, a positive shift of 0.82 nm is shown, with a bandwidth reduction from 56.01 nm, to 55.21; while for the profile 2, a positive shift of 0.60 nm with a bandwidth of 55.43 nm is recorded.

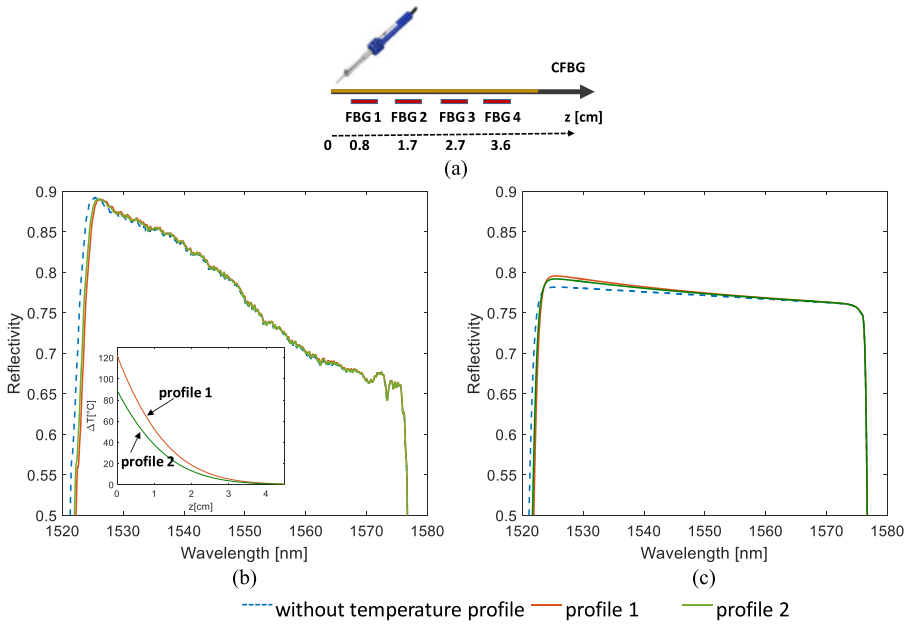

Fig. 10. Temperature gradient applied at the beginning of the CFBG sensor: (a) experimental scheme; (b) experimental CFBG response; (c) simulated CFBG response.

In conclusion, the sensitivity response trends for both the commercial CFBG sensor and the CFBG simulated sensor are comparable: in particular, for both, there is a small reduction in bandwidth when a temperature variation is applied at the beginning of the active part of the sensor.

In order to confirm the comparison between the simulated and experimental analysis, a second test was carried out on a different commercial CFBG sensor having the following characteristics: $L = 4$ cm; $\overline{\delta n_{eff}} = 7.8 \cdot 10^{-4}$; $\Lambda = 524$ nm, chirp rate $(d\lambda_D/dz) = 6.73$ nm/cm, $BW = 48$ nm (from 1521 nm to 1568 nm). The experiment was carried out with the same setup shown for the previous test (Fig. 9(a)): four standard FBG sensors 0.5 cm long, positioned in the same position with respect to the CFBG, as the previous test (see Fig. 11(a)).

In Fig. 11(b), it is reported the results of the test performed by applying a temperature profile at the center of the CFBG sensor.

In the inset of Fig. 11(b), they are shown the two temperature profiles applied, where their trend were obtained by the analysis of the response of the four standard FBG sensors used as a reference. In particular, the profile 1, applied at the center of the CFBG sensor, has a maximum temperature of 162 °C, while the profile 2, applied at the same point, has a maximum of 47 °C.

From the analysis of the commercial CFBG sensor response, it is noted that the application of a ΔT in the center of the grating, does not lead to changes in spectral edges and therefore no change in bandwidth. As expected from the simulation, the only change recorded is in reflectivity. Indeed, for profile 1, (with a maximum temperature of 162 °C), it is possible to observe the presence of a negative peak with a maximum of 0.75 at 1542 nm, and a positive peak, with a variation in the reflectivity of about 0.013 at 1550 nm, with respect to the spectrum without solicitation. Similar response is also observed for profile 2, where at 1542 nm there is a negative peak of about 0.76, and at 1550 nm a positive peak of about 0.77.

In Fig. 11(c), it is shown the CFBG sensor response simulated with the application of the two temperature gradients determined during the experimental tests (inset Fig. 11(b)). The application of these temperature gradients causes the formation of two peaks, one positive and one negative with the center of these peaks in correspondence of the maximum applied temperature; whereas no bandwidth variation is visible. In particular, for profile 1, a negative peak of 0.65, at the same wavelength observed for the experimental spectrum (1542 nm) is observed, with a variation in

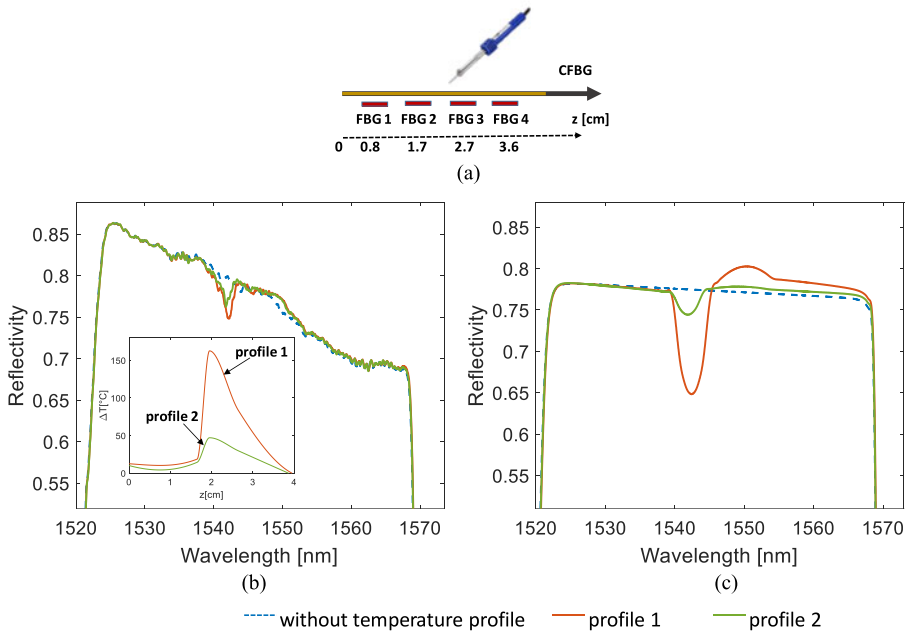

Fig. 11. Temperature gradient applied at the center of the CFBG sensor: (a) experimental scheme; (b) experimental CFBG response; (c) simulated CFBG response.

reflectivity of about 0.12 with respect to the spectrum without solicitation; a positive peak, less pronounced than the negative one, of 0.80 at 1550 nm is recorded. Similar behavior is observed for profile 2, but with a variation of reflectivity of about 0.03 and 0.01 at 1542 nm and 1550 nm respectively, compared to the spectrum without solicitation.

From the analysis of the experimental tests, we can state that the application of a positive ΔT leads to a positive shift at the point of application of the maximum temperature. If a positive temperature variation is applied to a limited part of the grating, this leads to a reduction in bandwidth, (as shown in the test reported in Fig. 10) on the contrary if a positive ΔT is applied along the whole length of the grating, an increase in bandwidth is shown. On the other hand, the application of a temperature profile at the center of grating, leads to the formation of two peaks and the possibility to precisely locate the point where the maximum temperature is recorded (at the center of the two peaks), without changes in the spectral edges.

5. Conclusion

In this paper, we used the TMM method to simulate CFBG sensors with the purpose of studying the contribution of the design parameters on the response of the sensor when subjected to thermal solicitation. Our goal was to simulate and analyze the CFBG sensor response to different temperature profiles in order to correlate spectral variations with the position of the thermal solicitation. In particular, from simulation data analysis, the length of the CFBG sensor should be selected according to the range of the monitored area and then selected for the specific application. Moreover, the length does not affect the thermal sensitivity of the sensor, so this parameter is only related to the application of interest.

Concerning the chirp parameter, it has been seen that for both linear and Gaussian profiles, for chirp values less than 3 nm/cm, the sensitivity of the sensor is very low, while for values between 5-6 nm/cm, highest sensitivity is reached, moreover also increasing the chirp value, the sensor maintains a good sensitivity useful for the biomedical purposes. Instead, the values of the λ_C (depending on the period and the chirp value chosen) and *BW* (depending on the period, the length and the chirp value chosen) are important for the choice of the spectrum position in the wavelength

range of interest, depending on the setup used and on the type of optical interrogator used. This kind of analysis is crucial for a proper design of CFBG sensor that leads to the best choice for the specific application.

Finally, experimental tests were performed, with simple temperature profiles applied, in order to demonstrate that is possible to measure the temperature along the grating length. The experimental results obtained are in accordance with the simulations. From the tests carried out, it is shown that, from the application of a temperature profile at the center of the grating, the bandwidth of the CFBG does not change. While it is evident the formation of two peaks (positive and negative) which allow to accurately locating the position of the maximum temperature peak.

These first results show the possibility of using this fiber sensor technology, to precisely monitor temperature variations, especially in applications where precision is below the millimeter would be required.

References

[1] A. Iadicicco, M. Della Pietra, G. Gaudio, and S. Campopiano, "Strain measurements of a multilayer panel via fiber Bragg gratings as novel approach for deflection monitoring of tracking particle detectors," *Proc. SPIE*, vol. 9506, 2015, Art. no. 95061L.

[2] A. Iadicicco, M. Della Pietra, M. Alviggi, V. Canale, and S. Campopiano, "Deflection monitoring method using fiber Bragg gratings applied to tracking particle detectors," *IEEE Photon. J.*, vol. 6, no. 6, Dec. 2014, Art. no. 0600610.

[3] S. J. Mihailov, "Fiber Bragg grating sensors for harsh environments," *Sensors*, vol. 12, no. 2, pp. 1898–1918, 2012.

[4] V. Mishra, N. Singh, U. Tiwari, and P. Kapur, "Fiber grating sensors in medicine: Current and emerging applications," *Sensors Actuators, A Phys.*, vol. 167, no. 2, pp. 279–290, 2011.

[5] P. Roriz, L. Carvalho, O. Frazão, J. L. Santos, and J. A. Simões, "From conventional sensors to fibre optic sensors for strain and force measurements in biomechanics applications: A review," *J. Biomech.*, vol. 47, no. 6, pp. 1251–1261, 2014.

[6] D. Tosi and G. Perrone, *Fiber-Optic Sensors for Biomedical Applications*. Norwood, MA, USA: Artech House, 2017.

[7] *Biological Evaluation of Medical Devices; International Organization for Standardization*, Geneva, Switzerland, ISO 10993, 1995.

[8] M. Ahmed, C. L. Brace, F. T. Lee, and S. N. Goldberg, "Principles of and advances in percutaneous ablation," *Radiology*, vol. 258, no. 2, pp. 351–369, 2011.

[9] E. Schena, D. Tosi, P. Saccomandi, E. Lewis, and T. Kim, "Fiber optic sensors for temperature monitoring during thermal treatments: An overview," *Sensors*, vol. 16, no. 7, 2016, Art. no. 1144.

[10] G. Palumbo *et al.*, "Temperature profile of *ex-vivo* organs during radio frequency thermal ablation by fiber Bragg gratings," *J. Biomed. Opt.*, vol. 21, no. 11, 2016, Art. no. 117003.

[11] S. A. Curley, "Radiofrequency ablation of malignant liver tumors," *Ann. Surg. Oncol.*, vol. 10, no. 4, pp. 338–347, 2003.

[12] P. F. Laeseke, F. T. Lee, L. A. Sampson, D. W. van der Weide, and C. L. Brace, "Microwave ablation versus radiofrequency ablation in the kidney: High-power triaxial antennas create larger ablation zones than similarly sized internally cooled electrodes," *J. Vascular Interventional Radiol.*, vol. 20, no. 9, pp. 1224–1229, 2009.

[13] Y.-F. Zhou, "High intensity focused ultrasound in clinical tumor ablation," *World J. Clin. Oncol.*, vol. 2, no. 1. pp. 8–27, Jan. 2011.

[14] E. M. Knavel and C. L. Brace, "Tumor ablation: Common modalities and general practices," *Tech. Vascular Interventional Radiol.*, vol. 16, no. 4, pp. 192–200, 2013.

[15] P. Saccomandi *et al.*, "Theoretical analysis and experimental evaluation of laser- induced interstitial thermotherapy in ex-vivo porcine pancreas," *IEEE Trans. Biomed. Eng.*, vol. 59, no. 10, pp. 2958–2964, Oct. 2012.

[16] D. Tosi, S. Korganbayev, N. Zhakin, R. Gassino, G. Perrone, and A. Vallan, "Towards inline spatially resolved temperature sensing in thermal ablation with chirped fiber Bragg grating," in *Proc. IEEE Int. Symp. Med. Meas. Appl.*, 2016, pp. 1–6.

[17] K. F. Chu and D. E. Dupuy, "Thermal ablation of tumours: Biological mechanisms and advances in therapy," *Nature Rev. Cancer*, vol. 14, no. 3, pp. 199–208, Feb. 2014.

[18] D. Tosi *et al.*, "Distributed fiber-optic sensors for thermal monitoring in radiofrequency thermal ablation in porcine phantom," in *Proc. Sensors*, 2014, pp. 39–42.

[19] D. Tosi, E. Macchi, G. Braschi, and M. Gallati, "Monitoring of radiofrequency thermal ablation in liver tissue through fibre Bragg grating sensors array," *Electron. Lett.*, vol. 50, no. 14, pp. 981–983, 2014.

[20] D. J. Webb, M. W. Hathaway, D. A. Jackson, S. Jones, L. Zhang, and I. Bennion, "First in-vivo trials of a fiber Bragg grating based temperature profiling system," *J. Biomed. Opt.*, vol. 5, no. 1, pp. 45–50, 2000.

[21] E. Samset, T. Mala, R. Ellingsen, I. Gladhaug, O. Søreide, and E. Fosse, "Temperature measurement in soft tissue using a distributed fibre Bragg-grating sensor system," *Minimally Invasive Therapy Allied Technol.*, vol. 10, no. 2, pp. 89–93, Jan. 2001.

[22] G. Palumbo *et al.*, "Fiber Bragg Grating for temperature monitoring during medical radiofrequency treatments," *Procedia Eng.*, vol. 168, pp. 1308–1311, 2016.

[23] G. Palumbo *et al.*, "Measurements of temperature during thermal ablation treatments on ex vivo liver tissue using fiber Bragg grating sensors," in *Proc. IEEE Int. Instrum. Meas. Technol. Conf.*, 2017, pp. 1–6.

[24] G. Palumbo *et al.*, "Real-time temperature monitoring during radiofrequency treatments on ex-vivo animal model by fiber Bragg grating sensors," *Proc. SPIE*, 2017, vol. 10231, Art. no. 102312K.
[25] P. Saccomandi, E. Schena, M. Diana, F. M. Di Matteo, G. Costamagna, and J. Marescaux, "Multipoint temperature monitoring in liver undergoing computed tomography-guided radiofrequency ablation with fiber Bragg grating probes," in *Proc. 38th Annu. Int. Conf. IEEE Eng. Med. Biol. Soc.*, 2016, pp. 5174–5179.
[26] T. J. Eom, M. J. Kim, B. H. Lee, and I. Chol Park, "Temperature monitoring system based on fiber Bragg grating arrays with a wavelength tunable OTDR," *IEICE Trans.*, vol. 88, pp. 933–937, 2005.
[27] R. Kashyap, *Fiber Bragg Gratings*, 2nd ed. Amsterdam, The Netherlands: Elsevier, 2010.
[28] I. R. Ivascu, R. Gumenyuk, and O. G. Okhotnikov, "Fabrication of high reflectivity chirped fiber Bragg gratings and its sensing applications," *Optoelentron. Adv. Mater. Commun.*, vol. 5, no. 9, pp. 911–915, 2011.
[29] D. Tosi, E. Schena, C. Molardi, and S. Korganbayev, "Fiber optic sensors for sub-centimeter spatially resolved measurements: Review and biomedical applications," *Opt. Fiber Technol.*, vol. 43, pp. 6–19, Jul. 2018.
[30] T. Erdogan, "Fiber grating spectra," *J. Lightw. Technol.*, vol. 15, no. 8, pp. 1277–1294, Aug. 1997.
[31] P. Saccomandi *et al.*, "Linearly chirped fiber Bragg grating response to thermal gradient: From bench tests to the real-time assessment during in vivo laser ablations of biological tissue," *J. Biomed. Opt.*, vol. 22, no. 9, pp. 1–9, Sep. 2017.
[32] I. Navruz and A. Altuncu, "Design of a chirped fiber Bragg grating for use in wideband dispersion compensation," in *Proc. 20th Int. Symp. Comput. Inf. Sci. New Trends Comput. Netw.*, 2005, no. 1, pp. 114–123.
[33] F. Ouellette, "Fiber Bragg gratings help WDM push limits of fiber capacity," *Laser Focus World*, vol. 34, no. 3, pp. 83–89, 1998.
[34] P. Bettini, E. Guerreschi, and G. Sala, "Development and experimental validation of a numerical tool for structural health and usage monitoring systems based on chirped grating sensors," *Sensors*, Basel, Switzerland, vol. 15, no. 1, pp. 1321–1341, 2015.
[35] Y. Okabe, R. Tsuji, and N. Takeda, "Application of chirped fiber Bragg grating sensors for identification of crack locations in composites," *Compos. Part A Appl. Sci. Manuf.*, vol. 35, no. 1, pp. 59–65, 2004.
[36] P. C. Won, J. Leng, Y. Lai, and J. A. R. Williams, "Distributed temperature sensing using a chirped fibre Bragg grating," *Meas. Sci. Technol.*, vol. 15, no. 8, pp. 1501–1505, 2004.
[37] D. Tosi *et al.*, "Fiber-optic chirped FBG for distributed thermal monitoring of ex-vivo radiofrequency ablation of liver," *Biomed. Opt. Express*, vol. 5, no. 6, 2014, Art. no. 1799.
[38] S. Korganbayev *et al.*, "Detection of thermal gradients through fiber-optic chirped fiber Bragg grating (CFBG): Medical thermal ablation scenario," *Opt. Fiber Technol.*, vol. 41, pp. 48–55, Mar. 2018.
[39] A. Othonos and K. Kalli, *Fiber Bragg Gratings: Fundamentals and Applications in Telecommunications and Sensing*. Norwood, MA, USA: Artech House, 1999.
[40] M. G. Xu, L. Dong, L. Reekie, J. A. Tucknott, and J. L. Cruz, "Temperature-independent strain sensor using a chirped Bragg grating in a tapered optical fibre," *Electron. Lett.*, vol. 31, no. 10, pp. 823–825, 1995.
[41] K. O. Hill and G. Meltz, "Fiber Bragg grating technology fundamentals and overview," *J. Lightw. Technol.*, vol. 15, no. 8, pp. 1263–1276, Aug. 1997.
[42] M. Prabhugoud and K. Peters, "Modified transfer matrix formulation for Bragg grating strain sensors," *J. Lightw. Technol.*, vol. 22, no. 10, pp. 2302–2309, Oct. 2004.
[43] M. Yamada and K. Sakuda, "Analysis of almost-periodic distributed feedback slab waveguides via a fundamental matrix approach," *Appl. Opt.*, vol. 26, no. 16, pp. 3474–3478, 1987.
[44] K. S. Khalid, M. Zafrullah, S. M. Bilal, and M. A. Mirza, "Simulation and analysis of Gaussian apodized fiber Bragg grating strain sensor," *J. Opt. Technol.*, vol. 79, no. 10, pp. 667–673, 2012.
[45] I. Navruz and A. Altuncu, "Design of a chirped fiber Bragg grating for use in wideband dispersion compensation," in *Proc. 20th Int. Symp. Comput. Inf. Sci. New Trends Comput. Netw.*, 2005, no. 1, pp. 114–123.